ADVANCED MATERIALS
www.advmat.de

How to Build Plasmon-Driven Molecular Jackhammers that Disassemble Cell Membranes and Cytoskeletons in Cancer

Ciceron Ayala-Orozco, Gang Li, Bowen Li, Vardan Vardanyan, Anatoly B. Kolomeisky,* and James M. Tour**

Plasmon-driven molecular machines with ultrafast motion at the femtosecond scale are effective for the treatment of cancer and other diseases. It is recently shown that cyanine dyes act as molecular jackhammers (MJH) through vibronic (vibrational and electronic mode coupling) driven activation that causes the molecule to stretch longitudinally and axially through concerted whole molecule vibrations. However, the theoretical and experimental underpinnings of these plasmon-driven motions in molecules are difficult to assess. Here the use of near-infrared (NIR) light-activated plasmons in a broad array of MJH that mechanically disassemble membranes and cytoskeletons in human melanoma A375 cells is described. The characteristics of plasmon-driven molecular mechanical disassembly of supramolecular biological structures are observed and recorded using real-time fluorescence confocal microscopy. Molecular plasmon resonances in MJH are quantified through a new experimental plasmonicity index method. This is done through the measurement of the UV–vis–NIR spectra in various solvents, and quantification of the optical response as a function of the solvent polarity. Structure-activity relationships are used to optimize the synthesis of plasmon-driven MJH, applying them to eradicate human melanoma A375 cells at low lethal concentrations of 75 nM and 80 mW cm^{-2} of 730 nm NIR-light for 10 min.

1. Introduction

Plasmons are the collective oscillation of the conduction band electrons in materials upon their optical excitation.[1] Optical plasmons can strongly absorb light, thereby concentrating their electric fields.[2,3] This has been exploited for a wide range of applications including optoelectronic devices,[4,5] sensors,[6–8] ultrasensitive analyte detection,[9,10] cancer theranostics,[11] solar energy harvesting,[12,13] water desalinization,[14] and photocatalysis.[15,16] Most of the research and applications of optical plasmons have been conducted in metallic or semimetallic nanomaterials.[17–19] In contrast, while molecular plasmons have been theoretically proposed, they have only recently been investigated experimentally.[20,21] Molecular plasmons couple the vibrational and electronic modes, resulting in concerted vibrational motion that is useful for mechanical work. Plasmon-driven motion had been described using energy transfer from a scanning tunneling microscopy tip to a zinc phthalocyanine adsorbed on a sodium chloride film, permitting the exciton formation and shuttling motion of the molecule.[22] The mechanism was attributed to i) direct energy tunneling into the molecule and electron–hole exciton formation and/or ii) nanocavity plasmon formation in between the tip and the substrate, permitting plasmon-driven energy transfer to the molecule for exciton formation, which then induces the shuttling motion. The authors did not attribute the excitation to that of a molecular plasmon intrinsic to the molecule. Based on experimental data and theoretical calculations, we recently showed that cyanine dyes support intrinsic molecular plasmon resonances upon near-infrared (NIR) light excitation, enabling mechanical permeabilization of cell membranes.[23] These molecules were termed molecular jackhammers (MJH) because the light-activated plasmons within the molecule coupled to a concerted whole-molecule vibration, leading to a vibronic-driven action (VDA). In our previous study,[23] the results support that mechanical action is a highly plausible working mechanism of the VDA in plasmon-driven MJH. We demonstrated how to distinguish the VDA mechanical effects from thermal and photochemical reactions. In short, the evidence is as follows: VDA is distinct from both photodynamic therapy and photothermal therapy in that the VDA mechanical effect on the cell membrane is not retarded by high doses of inhibitors of reactive oxygen species (ROS), and VDA does not itself induce an increase in the temperature of the media; it is also unaffected by

C. Ayala-Orozco, G. Li, B. Li, V. Vardanyan, A. B. Kolomeisky, J. M. Tour
Department of Chemistry
Rice University
Houston, TX 77005, USA
E-mail: ca5@rice.edu; tolya@rice.edu; tour@rice.edu
J. M. Tour
Department of Materials Science and Nano Engineering
the Smalley-Curl Institute
the Nano Carbon Center
and the Rice Advanced Materials Institute
Rice University
6100 Main St., Houston, TX 77005, USA

The ORCID identification number(s) for the author(s) of this article can be found under https://doi.org/10.1002/adma.202309910

DOI: 10.1002/adma.202309910

cooling the media to 2 °C. The photothermal effects are directly proportional to the absorption cross-section, molar extinction, and the concentration of the molecules or light-absorbing nanoparticles.[24] We differentiated the mechanical effects from photothermal effects by working at low concentrations (4 μM or lower) at light doses of 80 mW cm^{-2} for 10 min where the thermal effects were negligible. Evidence further supported this by comparing a strong MJH Cy7.5-amine with a weak MJH Cy7-amine, which has a higher molar extinction than Cy7.5-amine. Cy7-amine was much less efficient than Cy7.5-amine in opening cell membranes. The same behavior was observed in the comparison between a strong MJH Cy5.5-amine versus a weak MJH Cy5-amine. Regarding the photochemical reactions, we distinguished these effects from mechanical action by comparing the best MJH (Cy7.5-amine) with a cyanine molecule DiR (a lipophilic, near-infrared fluorescent cyanine dye), but a weak MJH that produced ≈20-fold higher concentrations of ROS, yet it did not permeabilize the cells. We further isolated the mechanical action from the ROS effects by studying MJH action on oxidation-resistant synthetic giant lipid vesicles and showed the stepwise mechanical opening.

Cyanine dye ICG has been reported as a photothermal and photodynamic agent to cause slow apoptotic cell death through oxidative stress.[25] In contrast, VDA of cell-associated MJH results in rapid necrosis (cell membrane disruption) within minutes. We showed that the photothermal effects of ICG start playing a role at concentrations above 8 μM where it causes a 1 °C temperature increase. ICG led to negligible cell membrane permeabilization in 0.8% of the cell population as observed with a 730 nm light dose of 80 mW cm^{-2} for 10 min.[23] A minor 2% permeabilization of cells was observed at 32 μM of ICG with a ≈3 °C increase. At 100 μM of ICG, only 13% of the cells were permeabilized with a ≈6 °C increase. For efficient photothermal killing of cancer cells using ICG in nanoparticle form, high light intensities (1 to 4 W cm^{-2}) and high concentrations of ICG (≈50 to 100 μM) are needed.[26,27] However, here we use cyanines as MJH in what is generally 50–100*x* lower concentration, with 10–50*x* lower optical powers than often used (80 mW cm^{-2} instead of 1 to 4 W cm^{-2}), exploiting its VDA mechanical effect to kill cells faster than with photothermal or photodynamic therapies.

Here we describe molecular plasmon modes in molecules and a method to quantify the plasmon resonance through a newly determined plasmonicity index. The plasmonicity index can be measured by recording the UV–vis–NIR spectra in a range of solvents and the trends of their resulting VDA can be predicted. We also exploit the use of NIR-light activated plasmons in a series of charged conjugated molecules to act as MJH to mechanically disassemble membranes and cytoskeletons in human melanoma A375 cells.

2. Results and Discussion

2.1. Building a Molecular Plasmon Library of Small Organic Molecules

MJH supports plasmon resonances in small organic molecules upon optical excitation. Here, four major resonances in cyanine-based molecular plasmons have been identified and proposed, supported by the induced charge density plots from density functional theory calculations in our recent work (**Figure 1**).[23] Two plasmon resonances are in the blue region of the visible spectrum and two are in the NIR region. These four plasmon resonances correspond to: 1) the dipolar oscillation of the electron density along the longitudinal axis of the molecule, called the longitudinal molecular plasmon (LMP); 2) the quadrupolar oscillation of electron density, primarily along the longitudinal axis and coupled with contributions along the transversal axis; 3) a quadrupolar oscillation of electron density, primarily along the transversal axis and coupled with contributions along the longitudinal axis; and 4) a dipolar oscillation of the electron density along the transverse axis, called the transversal molecular plasmon (TMP), as described in Figure 1A,B. A pictorial representation of the proposed mechanism of MJH to open cellular membranes upon NIR-light excitation is shown in Figure 1C,D. The optical excitation of plasmon resonances in MJH activates the electron density oscillations that simultaneously coupled with the nuclear vibrations, giving rise to VDA that can disassemble cellular membranes or supramolecular biological assemblies. The MJH associates with the lipid bilayers through hydrophobic and electrostatic interactions between the nonpolar portions and the polar substituents on the MJH, respectively. The phospholipids include phosphatidylglycerol, phosphatidylserine, phosphatidic acid, phosphatidylinositol, or cardiolipin, the latter shown in Figure 1D. Various molecules were synthesized by: 1) modifying the side chain that contributes to binding into lipid bilayers (Figure 1E); and 2) modifying the chemical structure of the conjugated core that strongly contributes to the plasmon resonance properties (Figure 1F–H). Following this strategy, a comprehensive library of MJH compounds was synthesized (**Figure 2**).

2.2. The Molecular Plasmonicity Index Correlates with the Cell Membranes Opening Activity

The activity of plasmon-driven MJHs to open cell membranes by VDA upon NIR light activation was evaluated in human melanoma A375 cells. When the cell membranes were opened by VDA, 4′,6-diamidino-2-phenylindole (DAPI), a blue-fluorescent dye that predominantly enters the cell when the lipid membrane is compromised, immediately stains the nucleus. Flow cytometry analysis was used to quantify the percentage of DAPI-positive cells at variable concentrations of MJH (Figures S1–S9, Supporting Information). The flow cytometry analysis was conducted immediately after the cells were treated with 730 nm LED light at 80 mW cm^{-2} for 10 min. Typically, it took ≈30 s to start cell counting and observe that DAPI had already entered the cell membrane-compromised cells but had not entered cells in the controls that did not have VDA. This is indicative of a rapid necrotic cell death and DAPI cell membrane permeabilization by VDA. The effective concentration needed to permeabilize 50% of the cells (VDA IC_{50}) was estimated for each molecule (Figures S10,S11, Supporting Information). To clarify, this method quantifies the opening of the plasma membrane since this is the physical layer through which DAPI enters the cell. Therefore, the concept of cell membrane permeabilization refers to the permeabilization of the plasma membrane. The

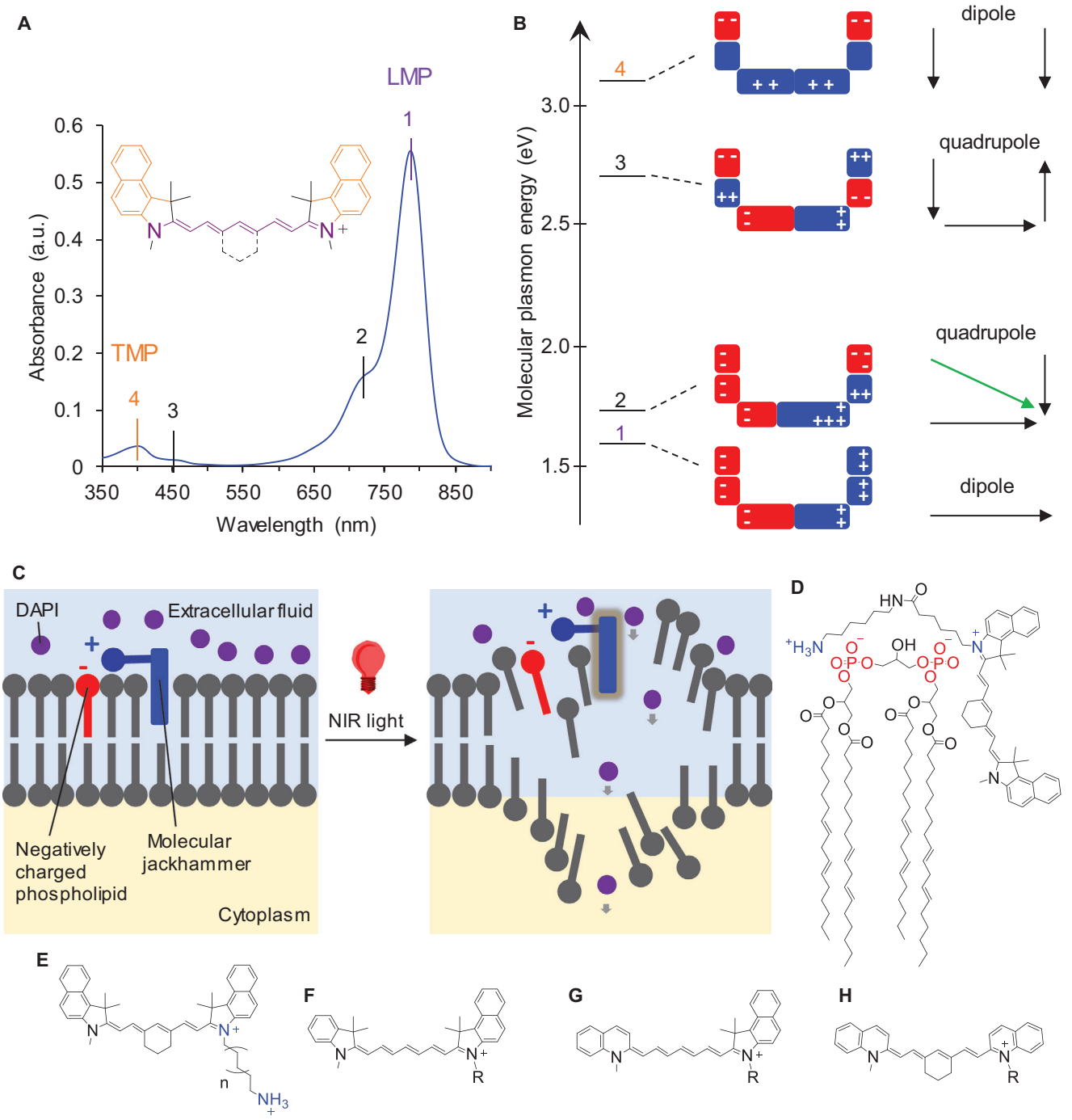

Figure 1. VDA model actuated by plasmon resonance. A) Absorption spectrum of cyanine-based MJH and assignment of four major molecular plasmon modes (1–4). The numbers 1–4 correspond to the levels 1–4 in B. The absorption shoulder 2 is the major vibronic mode (a concerted whole molecule oscillation of the plasmon longitudinally and transversally). Mode 1 is an LMP. The mode 4 is a TMP. B) The assignment of the four molecular plasmon modes to the corresponding pictorial model of the electron density distribution in the cyanine molecule. C) Mechanistic pictorial model of VDA to disassemble lipid bilayers. Step 1: Association of the MJH to the lipid bilayer. Step 2: Activation of VDA by NIR light to activate the molecular plasmons and vibrational modes in cyanine molecules. D) Proposed model of interaction between an aminocyanine and the negatively charged phospholipid cardiolipin (CL). Strategy to design structures of MJH E) by modifying the side chain, F) by removing the fused-benzene on the indole, or G,H) by substituting the indole with other resonant structures such as 1-methylquinoline.

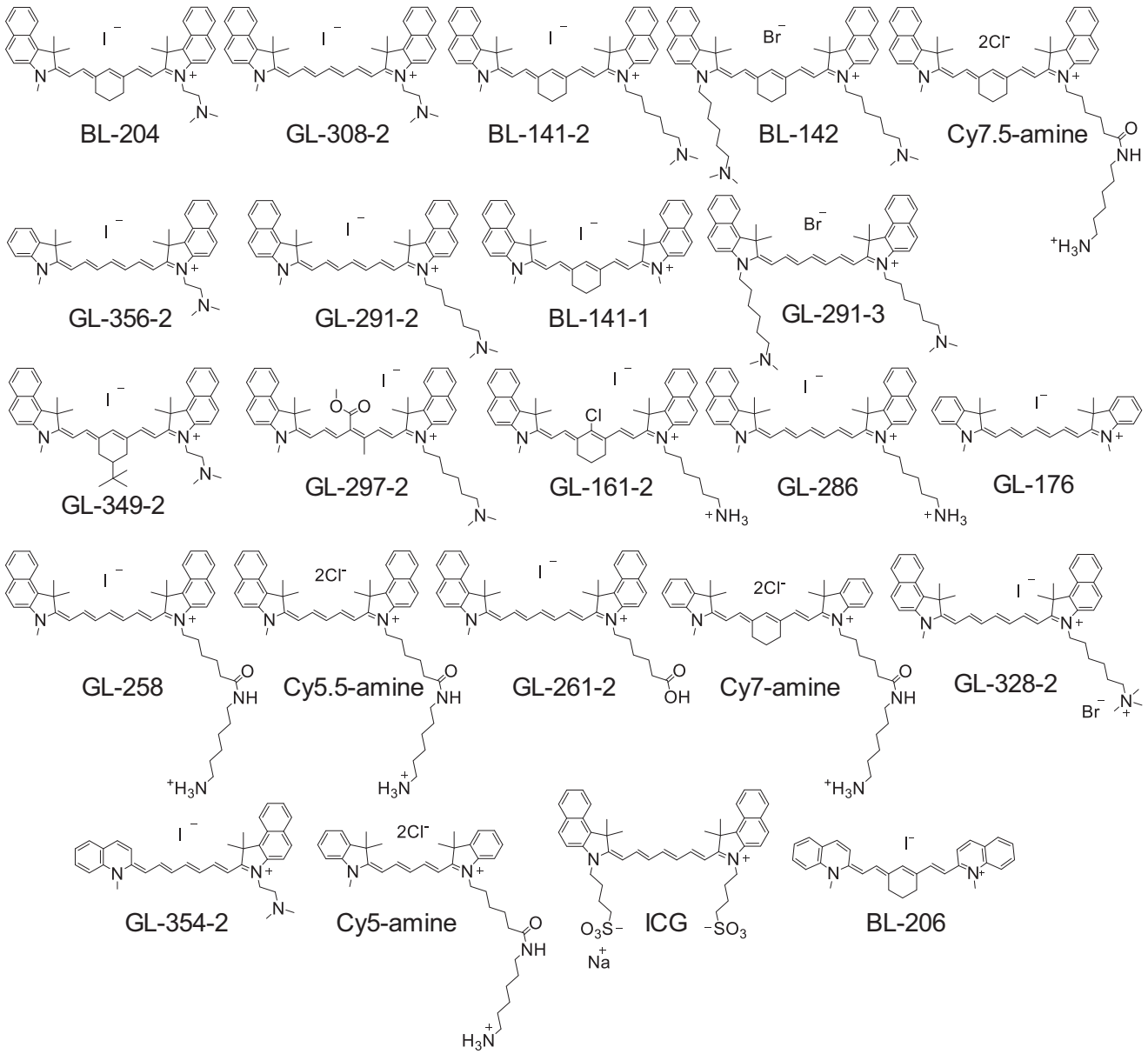

Figure 2. Chemical structures of cyanine-based MJH were built and used in this study. The structures are listed in descending order of VDA activity, top left to bottom right. The compounds listed as "Cy" or "ICG" are commercially available. The others were synthesized for this study.

library of MJH compounds was arranged from most active for BL-204 (VDA activity, VDA IC_{50} = 0.12 μM) to least active for BL-206 (VDA IC_{50} >> 8 μM) in Figure 2 and bottom to top in **Figure 3A**.

The VDA IC_{50} correlates with a new measurement that we disclose here called the "plasmonicity index". The experimental plasmonicity index (EPI) measurements are shown in Figure 3B–D. The EPI is a semiempirical experimental estimate of the plasmonic character of each molecule as shown in Figures S12,S13 (Supporting Information). The EPI is an estimate of the optical response of a molecular plasmon to the dielectric constant of the solvent, which reflects the plasmonic character of the molecule. This is done through the UV–vis–NIR spectral measurement of the MJH in isopropanol, ethanol, methanol, and water (Figures S14,S15, Supporting Information). The UV–vis–NIR absorbance is plotted as a function of the solvent polarity and the EPI is the slope of the linear correlation between the absorbance of the molecule against the dielectric constant of the solvent (Figures S12–S15, Supporting Information). Our method to measure EPI is highly reproducible and accurate when it is conducted using only pure solvents as shown in Figure S16 and Table S1 (Supporting Information). When solvent mixtures are included (water–methanol mixtures) new physicochemical effects appear to be introduced due to the molecular interaction between water and methanol as suggested by the results in Figure S16 (Supporting Information). The higher the EPI, the better the VDA activity to

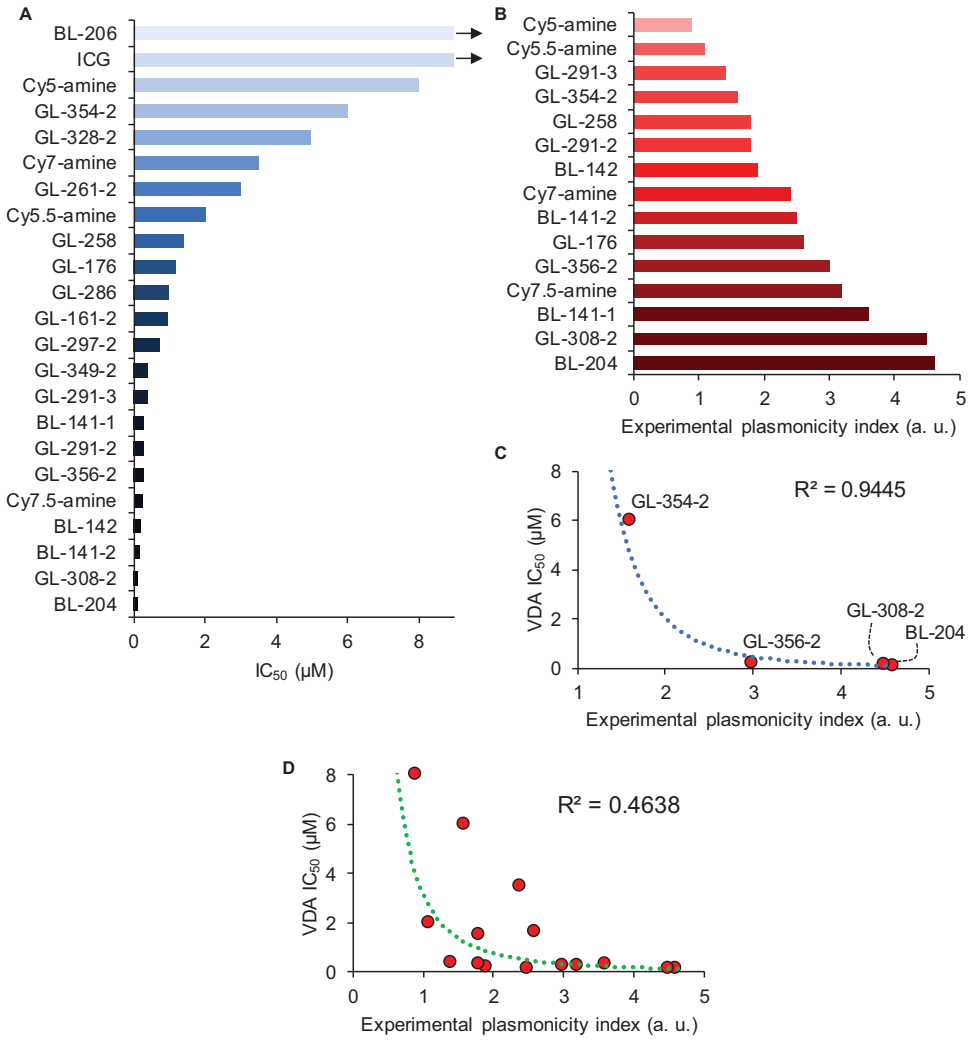

Figure 3. VDA to permeabilize human A375 melanoma cells using plasmon-driven MJH. A) Plasmon-driven MJH ordered by the effective concentration needed to permeabilize cells by 50% (VDA IC_{50}); BL-204 being the most active. The VDA IC_{50} of the most active molecule BL-204 is 0.12 μM. The IC_{50} in the least active molecules, BL-206 and ICG, are larger than 8 μm. Flow cytometry analysis was used to quantify the percentage of permeabilized cells using DAPI as a florescent stain for membrane-compromised cells. For this purpose, 10 000 cells were analyzed in each concentration as shown in Figures S1–S9 (Supporting Information) and plotted as concentration-response curves in Figures S10,S11 (Supporting Information). B) The compounds are ordered by the plasmonicity index, a parameter that estimates the VDA character in cyanine-based MJH. C) Correlation plot between the EPI and the VDA IC_{50} for a series of molecules with the same side chain but varied plasmonic core, BL-204, GL-308-2, GL-356-2, GL-354-2. We used the power function $y = a \times x^b$, $y =$ VDA IC_{50}, $x =$ EPI, $a = 25.82$, $b = -3.66$. D) MJH with varied side chains and varied plasmonic cores, plotted by their VDA IC_{50} versus the EPI to show the poor correlation when the effect of the side chain is convoluted with the effect of the plasmonic core. Light treatment consisted of 730 nm LED light at 80 mW cm^{-2} over 10 min, except for Cy5.5-amine and Cy5-amine, where a 630 nm LED was used to match the absorption of the plasmon resonance of the quadrupole mode in the NIR region.

permeabilize cells (Figure 3C). The correlation between EPI and VDA activity is clear when molecules with the same side chains, such as in BL-204, GL-308-2, GL-356-2, and GL-354-2, but variable plasmonic cores, are compared in Figure 3C. However, there is a poor correlation when both the side chains and the plasmonic cores are varied (Figure 3D) since the effect of the side chain is convoluted with the effect of the plasmonic core. This is the first attempt to quantify the relation between EPI and VDA activity. We used the power function $y = a \times x^b$ which provides a simple correlation between two quantities with a minimum number of variables where $y =$ VDA IC_{50}, $x =$ EPI, a and b are fitting coefficients. The side chains in the molecules strongly influence the binding of the MJH to the cell membranes as demonstrated by molecular dynamics (MD) simulations (**Figure 4**). The interaction of the MJH with the cell membrane is quantified by the depth of insertion and orientation (angle) within the lipid bilayer as is defined in Figure 4E. Different side chains influence the depth and orientation of the molecule within the lipid bilayer (Figure 4E–G). Therefore, we compared molecules with the same side chains and found a correlation: the higher the EPI, the better the VDA activity in all cases (Figures S17–S20, Supporting Information). In these comparisons, the structures of the side chains and the binding groups remain constant and only the core structure (plasmonic core) was varied.

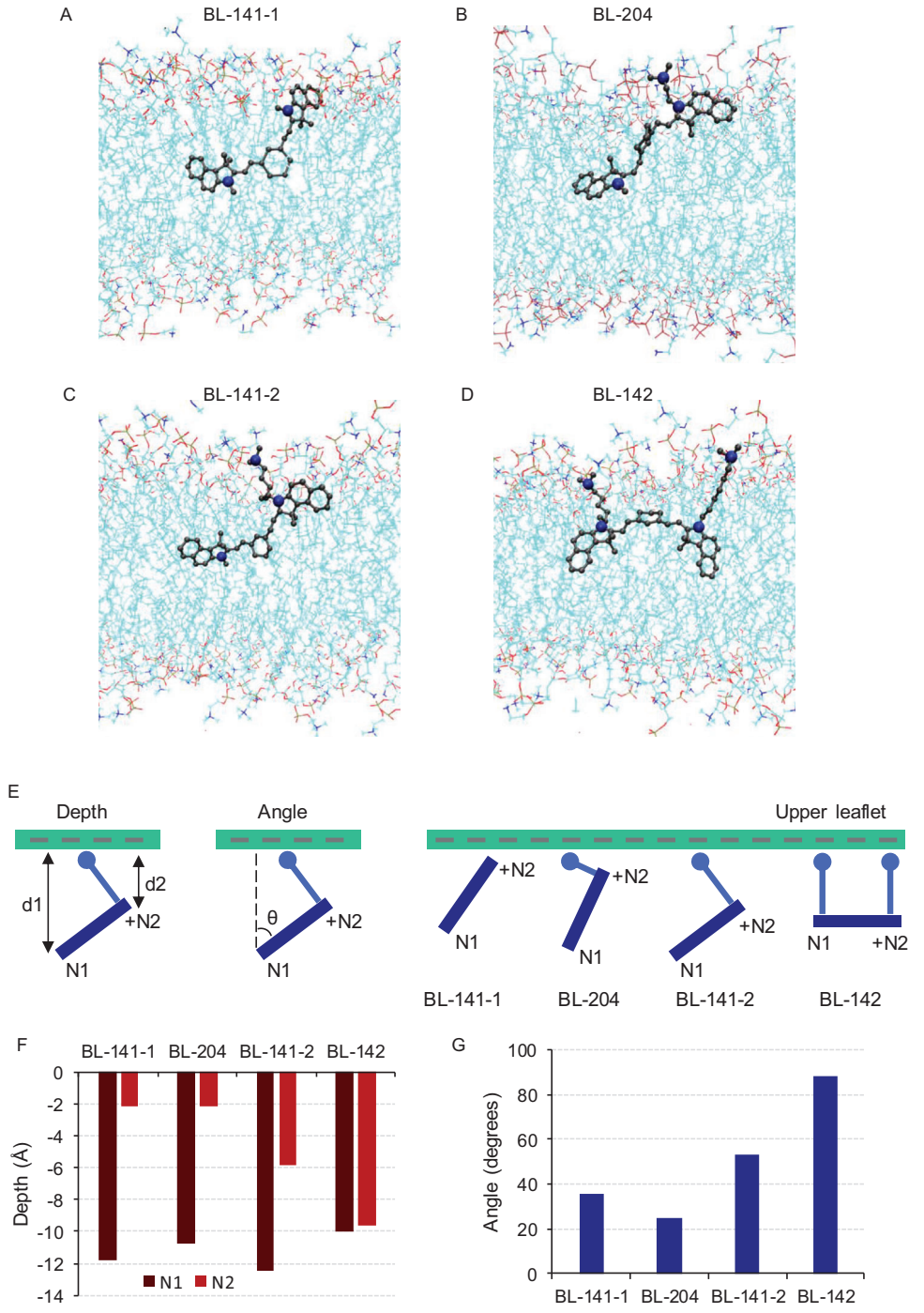

Figure 4. MD simulation of the effect of the side chain in the insertion of the MJH into lipid bilayers. Representative depiction of MJH bound to the lipid bilayers: A) BL-141-1, B) BL-204, C) BL-141-2, D) BL-142. E) Definition of quantitative parameters: the depth of the molecule in the lipid bilayer and the angle. The depth and angle are measured with respect to the position of the nitrogen atoms in the benzoindole: N1 represents the uncharged nitrogen and N2 represents the charged nitrogen. F) Average depth of the molecules within the lipid bilayers. N1 and N2 represents the positions of the nitrogen atoms as depicted in panel E. G) Average angle of the molecules within the lipid bilayer.

2.3. Estimation of the Concentration and the Force Exerted by MJH Over the Lipid Membrane

If all the MJH added into the cell suspension is bound to the plasma membrane, we have calculated that there are 1×10^5 MJH molecules bound per 1 μm^2 area of the plasma membrane for the case of BL-204 molecule (VDA IC_{50} = 0.12 μM) in 1 mL of 2×10^5 cells in suspension. This is considering an average surface area of 3500 μm^2 per cell, which was calculated from microscopy cell size measurements. To put this

into perspective, there are ≈2 × 10^6 phospholipid molecules in 1 μm^2 area of lipid bilayer.[28,29] Therefore, ≈5 molecules of MJH will be inserted in the lipid bilayer for every 100 lipid molecules.

The NIR 730 nm photon carries $E = hc/\lambda = 2.7 \times 10^{-19}$ J energy, where h is Planck's constant, and c is the speed of light. If all this energy is used for force generation, the generated force would be $F = E/s =$ 0.27 nN (considering the size s of the MJH molecule is ≈1 nm). Then, the total stress applied on the membrane is 270 mN m^{-1}. The mechanical stress required to rupture most membranes[30–32] is 1–30 mN m^{-1}. If only 10% of the energy carried by a 730 nm photon (F = 0.027 nN, stress = 27 mN m^{-1}) is used by the MJH for force generation, it would be enough to rupture the membrane. Indeed, the experimental measurement (Raman spectroscopy) of the concerted whole-molecule vibrational energy of MJH ranges from 164–171 meV (Figure S21, Table S2, Supporting Information). Then, for the whole-molecule vibration of a MJH with E = 164 meV, the calculated exerted force is ≈$F = E/s$ = 0.026 nN. Thus, the stress applied to the membrane is ≈26 mN m^{-1} which is enough to rupture the membrane. These are ultrafast concerted whole-molecule motions in the range of 40 THz (25 fs for a single excitation) that rupture the membrane (Table S2, Supporting Information).

2.4. Additional Photothermal and Photochemical Considerations

Previously, we have distinguished the MJH-mediated mechanical action through VDA from photothermal effects and photochemical reactions and the major findings are discussed in the introduction.[23] It is important to realize that the absorption of 730 nm light by MJH is nearly the same for the group of cyanines in this study when compared at the equal concentration (2.7 μM) as shown in Figures S14,S15 (Supporting Information). A photothermal mechanism could not explain the membrane opening activity since the photothermal effects are directly proportional to the light absorption cross-section (molar extinction) and the concentration of the molecules or light-absorbing nanoparticles.[24] Indeed, the light absorption intensity in water of the most VDA active molecule (BL-204) is among the lowest in the group. Furthermore, lower concentrations were sufficient for the most active MJH (VDA IC_{50} = 0.12 μM) to open cell membranes where the photothermal regime is negligible, thus further supporting the mechanical mechanism of action rather than photothermal.

Regarding the photochemical reactions, here we further explore that a high-concentration mixture of ROS scavengers (100 mM TU and 2.5 mM sodium azide)[23] cannot stop the MJH-mediated cell membrane permeabilization (Figure S22, Supporting Information). Four MJH were evaluated (BL-204, GL-308-2, BL-141-2 and BL-142) in two independent experiments (n = 2). The results further suggest that the photochemical reactions are less likely responsible for the rapid permeabilization of cell membranes within 10 min or less. Instead, others have shown that the photochemical reactions by cyanines caused slow apoptotic cell death through oxidative stress.[25] Overall, the evidence continues to support that MJH-mediated cell membrane opening through VDA is likely different than photothermal and photochemical mechanisms.

2.5. Guidelines to Design and Synthesize Plasmon-Driven MJH

Having identified quantitative parameters, the EPI, and VDA activity, we outline the guidelines to build more active plasmon-driven MJH. 1) The C6-ring in the polymethine bridge increases the plasmonicity and VDA activity to permeabilize cells (Figure S17, Supporting Information). This effect is presumably due to the C6-ring increasing the rigidity of the polymethine bridge, allowing better conjugation and thereby oscillation of the electron density along the longitudinal axis of the molecule. 2) The length of the polymethine bridge influences the plasmonicity and thereby the vibronic effect to permeabilize cells (Figure S18, Supporting Information). The longer the π-conjugation, the higher the plasmonicity index. This is consistent with theoretical calculations that predict that the plasmonicity index should be directly proportional to the number of atoms in polyaromatic hydrocarbon systems.[33] 3) The addition of a fused benzene ring to the indole increases the plasmonicity and thereby the VDA activity because it increases the π-conjugation and the number of atoms that can support the plasmon oscillation (Figure S19, Supporting Information). In contrast, the lack of fused benzene moieties such as in Cy7-amine and Cy5-amine limits the molecular plasmon oscillation of the electron density in the transverse direction. The weak TMP resonance is observed in the UV–vis spectrum of Cy7-amine at ≈380 nm in Figure S14 (Supporting Information) and Cy5-amine at ≈320 nm in Figure S15 (Supporting Information). 4) Substitution of the indole by other alternative resonance structures, such as 1-methylquinoline, weakens the plasmonicity and the VDA activity (Figure S20, Supporting Information). Like point 3, the 1-methylquinoline limits the oscillation of the electron density along the transverse axis of the molecule as shown by the weak TMP in the UV–vis spectrum of BL-206 at ≈370 nm in Figure S15 (Supporting Information). The position of the maximum absorption wavelength for the peak, a dipolar LMP mode, and the shoulder, a quadrupolar vibronic mode, split when measured in water as shown by the spectrum of BL-206 in Figure S15 (Supporting Information). This suggests that the indole promotes a strong coupling of longitudinal and transversal electron density oscillation in cyanine-based molecular plasmons while the 1-methylquinoline hinders the coupling. 5) The addition of electron-withdrawing substituents such as *N*, *N*-dimethylamine within two carbon atoms of the nitrogen of the benzoindole strongly improves the plasmonicity and VDA activity. The compounds with this structural element, BL-204 and GL-308-2 (Figure 2), are the top performers in the library of compounds. The *N*, *N*-dimethylamine might be producing a charge perturbation that induces charge transfer in the system, leading to the formation of stronger coupling between the longitudinal dipolar and quadrupolar molecular plasmon modes (Figure S14, Supporting Information), analogous to the effect in plasmonic gold nanoparticles that can be perturbed by a small gold sphere attached to the nanoparticle.[34] This effect is observed in BL-204 and GL-308-2, Figure S14 (Supporting Information) when the absorption peak of the dipolar LMP diminished significantly in water and partially merged with the shoulder into a single peak. This occurs because the energy level of the dipolar LMP and the quadrupolar vibronic mode, the shoulder in the spectrum, approaches degeneracy by the perturbation of the protonated *N*, *N*-dimethylamine in water.

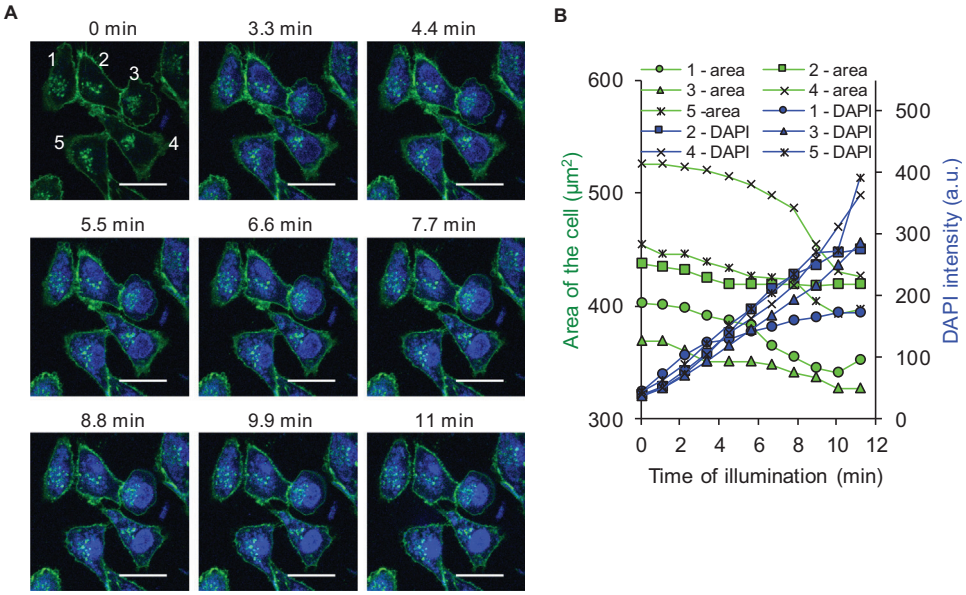

Figure 5. The effect of plasmon-driven MJH Cy5.5-amine on disassembling cellular membranes and cytoskeleton upon NIR-light activation. A) Images of A375 cells recorded over time under treatment with Cy5.5-amine and 640 nm light exposure. Loading concentration of Cy5.5-amine: $C_{loading}$ = 4 μM for 45 min. CellMask Green is added to visualize the plasma membrane in green, loading concentration $C_{loading}$ = 5 μg mL^{-1} for 30 min, λ_{ex} = 488 nm, and λ_{em} = 500–550 nm. The 640 nm light exposure times are shown on the top of each image. The numbers on the panel at time = 0 min is to label the cells under analysis. B) The area of the cell and the permeabilization of DAPI into A375 cells was recorded over time. The area of the cells shows that the cytoskeleton is shrinking upon activation of the VDA in Cy5.5-amine. The DAPI staining indicates the permeabilization of the plasma membrane. Loading concentration of DAPI: $C_{loading}$ = 1 μM, λ_{ex} = 405 nm, and λ_{em} = 425–475 nm. The controls: a) exposure to light alone, b) exposure to Cy5.5-amine alone, and c) blank are shown in Figures S26–S28 (Supporting Information). Scale bar = 25 μm. The photoactivation consisted of exposure to a 640 nm confocal microscope laser at 25% power (250 μW power, HV (gain) = 100, dwell time per pixel = 2.18 μs, Plan Apo IR 60*x*/1.27 water immersion objective).

2.6. MJHs Targets Mitochondria, Outer Cellular Membranes, and Nuclear Membranes in A375 Cells

Cyanines are photostable high-quantum yield fluorescent probes whose physical characteristics provide a simple method to determine their cellular localization by confocal microscopy (Figure S23, Supporting Information).[35,36] The MJH in this study tend to associate with the cellular membranes. The side chains in the cyanine-based MJH influence their permeability into specific cellular membranes. It was observed that Cy5.5-amine binds to the outer cell membrane, the nuclear membrane, and the mitochondria (Figure S23, Supporting Information). The same binding pattern was observed for Cy7.5-amine, Cy7-amine, Cy5-amine in our former study, exemplifying that cyanines with the same side chain bind in similar ways into the cellular membranes.[23] This further justifies that the correlation between VDA-mediated activity and EPI should be studied within groups of molecules with the same side chain to keep the binding mode as a constant variable as shown in Figure 3C and Figures S17–S20 (Supporting Information). The mitochondria targeting is presumably through a docking interaction with cardiolipin, a phospholipid that is present exclusively in the internal lipid bilayer of mitochondria. This is supported by the flow cytometry analyses in Figure S24 (Supporting Information),[37–39] which shows that free cardiolipin added in the medium interacts with Cy5.5-amine and competes with the binding of Cy5.5-amine to the cancer cells.

2.7. Plasmon-Driven MJH Cy5.5-Amine Disassembles Cellular Membranes and Cytoskeleton Upon NIR-Light Activation

The plasmon resonance in Cy5.5-amine was activated upon laser excitation (λ_{ex} = 640 nm) under the confocal microscope while imaging the real-time opening of the outer cellular membrane. DAPI enters the cell through the openings, thereby staining nuclear DNA. The cytoskeleton was simultaneously disassembling (**Figure 5**, Movie S1, and Figure S25, Supporting Information). These effects are not observed in the controls with light treatment only (Figure S26, Supporting Information), MJH only (Figure S27, Supporting Information) or without treatment (Figure S28, Supporting Information). The plasmon-driven MJH disassembled the plasma membranes, and pieces of the cell membrane broke apart from the cell as observed in Movie S1 (Supporting Information) in real-time and in Figure S29 (Supporting Information). Simultaneously, it was observed that the cells were shrinking in size (Figure 5; Figure S25, Supporting Information). This cell shrinkage was quantified as the area defined by the perimeter of the outer cell membrane over time (Figure 5; Figures S25–S28, Supporting Information). The shrinkage of the cell results, because the cytoskeleton was contracting, as determined in a similar experiment, imaged using green fluorescent protein-labeled actin (Figure S30, Supporting Information). This suggests that the cytoskeleton is disassembling while simultaneously the plasmon-driven MJHs are destroying cellular membranes. The light alone does not cause the shrinking of the cell

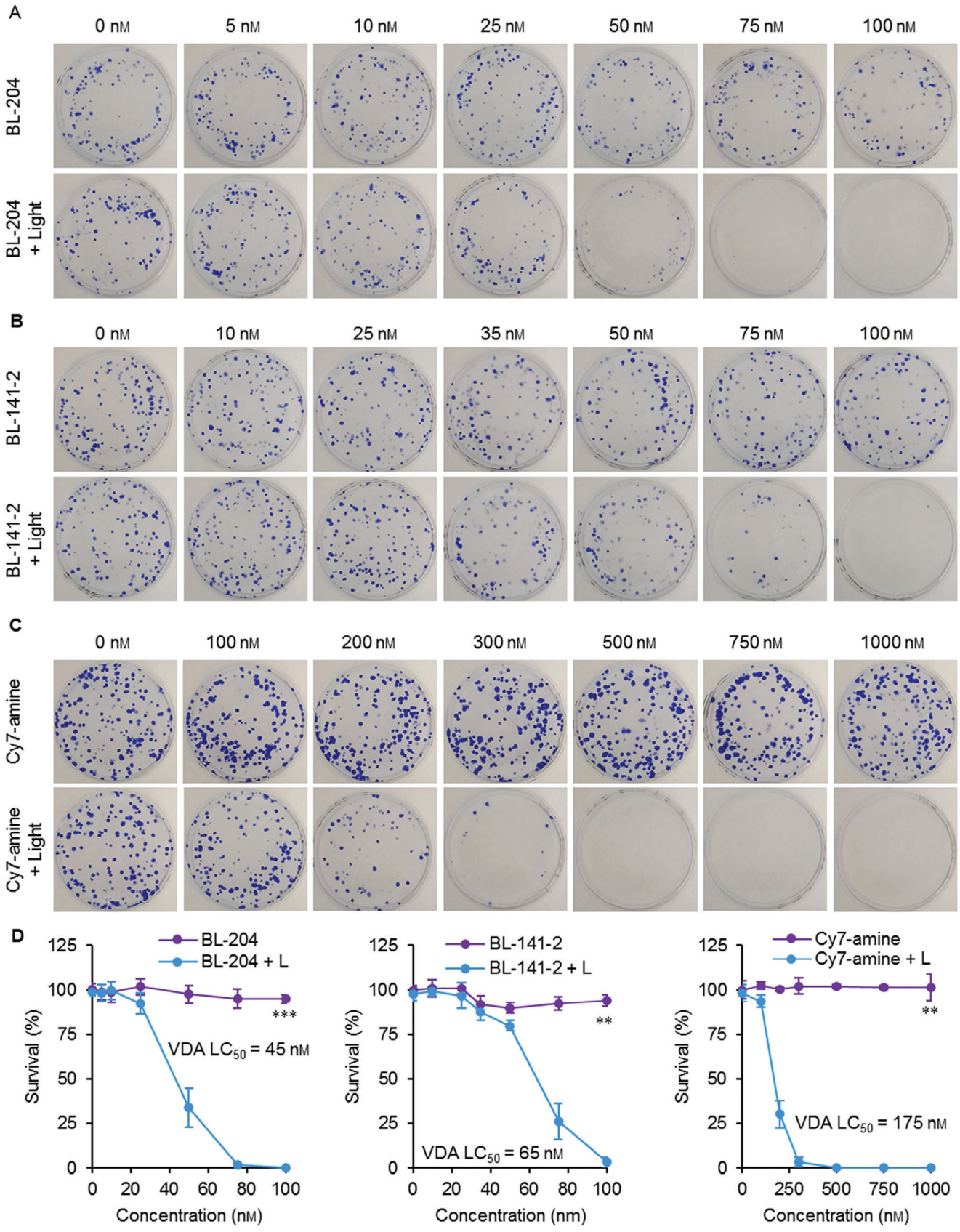

since no DAPI enters (Figure S26, Supporting Information). Instead, the cells respond to the light alone and have time to maintain control of their movement because they are not being destroyed. It is presumed the cells were moving away from the light since we observed a slight increase in the cells' area (Figure S26, Supporting Information). This is additional evidence that the VDA in plasmon-driven MJH is producing mechanical action that is different than the action induced by light alone. The MJH without light activation has no effect on the area of the cell nor does DAPI enter the cell within the time window of the experiment (Figure S27, Supporting Information). These changes are not observed in the cells without any treatment; only CellMask Green was added to visualize the cell membrane and DAPI to measure the integrity of the cell membrane (Figure S28, Supporting Information).

2.8. Lethal Concentration of Plasmon-Driven MJHs

A clonogenic assay was conducted to confirm that cancer cells treated by plasmon-driven MJH are killed upon NIR-light activation (**Figure 6**). Three molecules were tested: the most VDA active BL-204, the medium VDA active BL-141-2, and the low VDA active Cy7-amine. The lethal concentration to kill the cell population by 50% (VDA IC_{50}) was found to be 45, 65, and 175 nM, respectively. The lethal concentrations to eradicate 100% of the cancer cells were 75, 100, and 500 nM, respectively. This result confirms that BL-204 is one of the most active compounds in this library to eradicate cancer cells. This was accomplished by incubating the MJH molecules with the A375 cells for 50 min and then activation of the plasmon-driven MJH using 730 nm NIR-light at 80 mW cm^{-2} for 10 min.

2.9. Predicted Octanol–Water Partition Coefficient (logP Value) in Cyanine-Based MJH

To determine if the higher cell membrane permeabilization activity was simply due to higher cell membrane affinity rather than the EPI, we calculated the octanol–water partition coefficient, logP value, of the MJH using a logP calculator. This parameter indicates the lipophilicity of the MJH to the lipid bilayers.[40,41] The higher the value the more likely the MJH will bind to the lipid bilayers. The protonation state of the MJH strongly influences the polarity of the molecules and hence the logP values. The logP values were calculated considering the charged state (amine protonated or carboxylic acid ionized) of the side chain (Figure S31A, Supporting Information) or in the neutral state (Figure S31B, Supporting Information) if no ionization was presumed. The charged state is more likely to occur at pH ≈7.4 in the medium since the pKa of the deprotonation of alkyl amines is ≈9.5–11 and of the ionization of the carboxylic acid is ≈5. The logP values do not fully correlate with the ability to permeabilize cell membranes (Figure S31C,D, Supporting Information). This supports the finding that the affinity of MJH to cell membranes is not the main factor responsible for VDA-mediated cell membrane permeabilization. There are highly VDA active MJH such as BL-204, GL-308-2, and GL-356-2 with relatively low logP values. In contrast, there are molecules such as BL-141-1 and BL-142 with relatively high logP values that should have high concentrations in the lipid bilayers but are not the most VDA active. This is evidence that the VDA activities are not simply due to the amount of MJH bound into the lipid bilayers but include the plasmon-mediated action that defines the VDA activity.

The lack of full correlation between logP values and VDA activity does not mean that the binding of MJH into the lipid bilayers is not playing a role. In a select group of molecules, ICG, GL-328-2, GL-286, and GL-291-2, the logP values correlate well with the VDA activity (Figure S32, Supporting Information). This correlation might exist because the molecules have the same plasmonic core structure and the same alkyl chain length, although they have different alkyl chain functional groups.

Molecules BL-204 and GL-308-2 have low logP values but the highest VDA activities for permeabilizing cell membranes (Figures S33,S34, Supporting Information) and the highest plasmonicity index (Figure S12, Supporting Information), evidence that molecular plasmon is responsible for the VDA-mediated cell membrane permeabilization. Possibly, the protonated secondary amine, close to the core plasmonic structure, causes the moiety to act as an electron-withdrawing group to enhance its plasmonicity.

2.10. Some MJH Preferentially Target Mitochondria While Others Target the Endoplasmic Reticulum (ER)

The specific localization of the MJH was studied by fluorescence confocal microscopy using MitoTracker, a marker for localization in mitochondria; ER-Tracker, a marker for localization in ER; and CellMask, a marker for localization in the outer cell membrane; in Figures S35–S38 (Supporting Information). A group of MJH preferentially localized in mitochondria: Cy5.5-amine, Cy7-amine, GL-261-2, BL-242, and BL-141-2. Other MJH preferentially localized in the ER: GL-308-2 and BL-142. BL-141-1 did not show preferential localization. This can explain the differences in VDA activity that we observe in BL-141-2, BL-142, and BL-141-1. In these three compounds, there is no correlation between the VDA activity, the plasmonicity index, or the logP values. This suggests that the selective binding of these compounds within the cell membranes is playing a major role in the VDA activity. This is supported by MD simulations that predict different binding modes for BL-141-2, BL-142, and BL-141-1 in which the structural variation is only in their side chains (Figure 4).

Figure 6. Lethal concentration of plasmon-driven MJHs at short contact time (50 min) in A375 cells. Clonogenic assay was conducted in the presence of A) MJH BL-204, B) MJH BL-141-2, and C) MJH Cy7-amine. D) Quantification of the surviving cells and estimation of the lethal concentration to kill 50% of the cells (VDA LC_{50}). Letter L stands for light treatment. A375 cells were incubated with the molecules for 50 min, and then treated with light (730 nm at 80 mW cm^{-2} for 10 min). Immediately after the treatment the molecules in the media were removed by exchanging with clean media and then the cells were cultured for colony formation over 7 days. The clonogenic assay was conducted in triplicate ($n = 3$, biological replicates). Data are presented as mean values +/- SEM. *t*-test paired two samples for means, two-tail, * $p < 0.05$, ** $p < 0.01$, *** $p < 0.001$, statistical significance $p < 0.05$. The exact p values obtained were $p = 0.0007$ (for BL-204 vs BL-204 + L at 100 nM), $p = 0.003$ (for BL-141-2 vs BL-141-2 + L at 100 nM), and $p = 0.005$ (for Cy7-amine vs Cy7-amine + L at 1000 nM).

2.11. The Effect of Contact Time on the Cytotoxicity of MJH Using a Crystal Violet Test

The contact time during the incubation of MJH with A375 cells has a strong effect on the cytotoxicity. Generally, MJH at a short contact time (≈40 min) showed little to no cytotoxicity (Figure S39, Supporting Information). However, at long contact time (1 or 2 days) MJH became toxic, likely through a slow cytotoxic mechanism. Interestingly, in some cases, we have observed that MJH such as GL-261-2 can increase the cell viability at short contact time as shown in Figure S39C (Supporting Information) and GL-286 at low concentrations (<1 μM) as shown in Figure S39D (Supporting Information). For the short contact times of 40 or 50 min, the MJH was incubated with A375 cells, then the excess was removed by centrifugation, and the cells were cultured for 2 d. The cell viability was then measured by a crystal violet test. For the long contact time, the MJH were incubated with A375 cells for 1 or 2 days and then the viability was immediately measured by a crystal violet test (Figures S40,S41, Supporting Information). The mild effects at short contact time (≈40–50 min) are through a slow cell killing mechanism, likely apoptosis since the more complete killing is observed after culturing the cells for 2 days. This contrasts with the necrotic cell death induced by NIR-light-activated VDA that takes 10 min to kill the cells. These are two distinctive, and in some aspects opposing, mechanisms of action for cell death.[42,43]

The question that arises regarding the MJH cytotoxicity without light activation is: Does the MJH toxicity directly correlate to the VDA activity? To answer this question, we built 2D correlation plots comparing the VDA activity under light activation versus the toxicity of the molecules without light activation (Figure S42, Supporting Information). There is no direct correlation between the VDA activity and inherent toxicity. More importantly, BL-142, with relatively low inherent toxicity with respect to others, retains high VDA activity. The VDA activity was measured by flow cytometry at 10 min immediately after light treatment while the inherent toxicity was measured by crystal violet test after continuous MJH exposure to the cells for 2 days.

2.12. The Effect of Contact Time in the Cytotoxicity of MJH Using Clonogenic Assay

For additional assessment of the VDA activity versus the inherent toxicity, both properties were measured using a clonogenic assay for cell viability. The exposure time in both experiments was equal (Figure S43, Supporting Information), 7 h for both, followed by culture of the cells for 7 days to allow colony formation. The cell survival was calculated at the end of the colony formation (Figures S44,S47, Supporting Information). Lower inherent toxicity molecules from Figure S42 (Supporting Information) were included in the analysis; additional molecules were synthesized seeking to reduce their inherent toxicity. For example, from Figure S42 (Supporting Information) we identified that the carboxylated GL-261-2 was less toxic than the aminocyanines. Following this observation, we synthesized BL-242 (Figure S43E, Supporting Information). The acetylation of the amine such as in GL-362-2 enhanced the toxicity (Figure S43E, Supporting Information). Overall, no direct correlation between the light-activated VDA activity, and the inherent toxicity was observed (Figure S43A vs Figure S43B, Supporting Information). The ratio of inherent toxicity/VDA activity was defined to identify the lead molecule with the highest therapeutic index of VDA activity versus inherent toxicity (Figure S43C, Supporting Information). Specifically, the therapeutic index was defined as the ratio of Tox LC_{50}/VDA LC_{50}. BL-141-2 has a convenient high therapeutic index of 22 and a very low VDA LC_{50} = 18 nM to eradicate 50% of the cells and VDA LC_{100} = 40 nM to eradicate 100% of the cells. GL-261-2 is the lead molecule with the highest therapeutic index of 62 and a VDA LC_{50} = 80 nM (Figure S43D, Supporting Information). GL-261-2, with a therapeutic index of ≈60, is a plasmon-driven MJH candidate for translation to rodent studies, which is safer than Cy7.5-amine (therapeutic index of ≈2–5 depending on the method used) that was successfully applied in vivo to eradicate melanoma tumors without signs of toxic side effects in mice.[23]

3. Conclusion

A library of 23 NIR 730 nm light-activated MJH displaying plasmon-driven vibrational action was designed and synthesized (Figures 1,2). This library was originally screened for the membrane permeabilization of human melanoma A375 cells by VDA upon NIR-light activation, allowing the identification of structural elements that improve the plasmon-driven activity (Figure 3). A cyanine, BL-204, was the best MJH to permeabilize cellular membranes. The contribution of each structural element to the plasmonicity of the molecule was quantified by its EPI (Figures S12,S13, and S17–S20, Supporting Information). The plasmonicity was improved by synthesizing molecules such as GL-308-2 and BL-204 (Figure S12, Supporting Information).

The EPI is a method described here to quantify the effects of molecular structure on the activity of the MJH. The theoretical plasmonicity index, based on complex quantum mechanical calculations, has been described elsewhere.[44,45] The EPI correlates with the VDA activity when comparing MJH with the same side chains but variable cores (Figure 3C; Figures S17–S20, Supporting Information).

MJH Cy5.5-amine binds to the cellular membrane, nuclear membrane, and mitochondria (Figure S23, Supporting Information). In the mitochondria, the protonated Cy5.5-amine most likely docked in the lipid bilayer to the negatively charged cardiolipin, a phospholipid exclusively localized in the internal mitochondrial membrane, as supported by the flow cytometry competitive assay (Figure S24, Supporting Information). Similar molecules such as Cy7.5-amine, Cy7-amine, Cy5.5-amine, and Cy5-amine should also dock into the lipid bilayers. It was confirmed that Cy7-amine targets localization in cellular membranes like Cy5.5-amine (Figure S35, Supporting Information). This is supporting evidence that MJH with similar side chains target similar sub-cellular organelles.

Plasmon-driven MJH was utilized to destroy cellular structures; this characteristic can be applied to cancer treatment and the destruction of bacteria, fungi, and viruses.[46,47] The plasmon-driven MJH might be active in other biomedical applications by tuning the NIR-light power intensity and exposure time to the optimal levels for modulation of biological activity, such as cell signaling or selective opening of protein channels.[48] Since these MJH are activated in the NIR, they reside in the therapeutic

window that permits efficient light penetration through biological tissue, serving as a harbinger for future medical applications of molecular machines.

Supporting Information

Supporting Information is available from the Wiley Online Library or from the author.

Acknowledgements

The authors are thankful to Prof. H. Xiao at Rice University for kindly hosting C.A.O. and sharing his laboratory to culture the A375 cancer cells. The authors thank Dr. D. James for editing the manuscript. The authors also thank Dr. A. B. Utama for confocal microscopy training and Dr. H. Deshmukh for flow cytometry training at the Rice Share Equipment Authority. J.M.T. acknowledges financial support from The Discovery Institute and The Welch Foundation (C-2017-20220330).

Conflict of Interest

Rice University owns intellectual property on the use of MJH coupled with VDA for the permeabilization of cell membranes. Nanorobotics Ltd. is the possible licensee of this technology from Rice University. J.M.T. is a stockholder in Nanorobotics Ltd., but not an officer, director, or employee. Conflicts are mitigated through regular disclosure to and compliance with the Rice University Office of Sponsored Programs and Research Compliance. The authors declare no other potential conflicts.

Author Contributions

C.A.O., G.L., and B.L. contributed equally to this work. C.A.O. and J.M.T. conceptualized the idea. C.A.O. conducted biological studies, plasmon physics, and spectroscopy. G.L. and B.L. conducted the chemical synthesis of the MJH library. V.V. conducted the theoretical calculations and simulations under the supervision of A.B.K. J.M.T. was responsible for the funding acquisition and project supervision. C.A.O. and J.M.T. wrote the original draft. All authors reviewed, wrote, and edited the final manuscript.

Data Availability Statement

The data that support the findings of this study are available in the supplementary material of this article.

Keywords

cancer, mechanical, molecular jackhammers, molecular machines, molecular plasmons

Received: September 24, 2023
Revised: December 19, 2023
Published online: January 6, 2024

[1] E. Prodan, C. Radloff, N. J. Halas, P. Nordlander, *Science* **2003**, *302*, 419.
[2] N. J. Halas, S. Lal, W.-S. Chang, S. Link, P. Nordlander, *Chem. Rev.* **2011**, *111*, 3913.
[3] J. A. Schuller, E. S. Barnard, W. Cai, Y. C. Jun, J. S. White, M. L. Brongersma, *Nat. Mater.* **2010**, *9*, 193.
[4] E. Ozbay, *Science* **2006**, *311*, 189.
[5] H. A. Atwater, A. Polman, *Nat. Mater.* **2010**, *9*, 205.
[6] J. Langer, D. Jimenez De Aberasturi, J. Aizpurua, R. A. Alvarez-Puebla, B. Auguié, J. J. Baumberg, G. C. Bazan, S. E. J. Bell, A. Boisen, A. G. Brolo, J. Choo, D. Cialla-May, V. Deckert, L. Fabris, K. Faulds, F. J. García De Abajo, R. Goodacre, D. Graham, A. J. Haes, C. L. Haynes, C. Huck, T. Itoh, M. Käll, J. Kneipp, N. A. Kotov, H. Kuang, E. C. Le Ru, H. K. Lee, J.-F. Li, X. Y. Ling, et al., *ACS Nano* **2020**, *14*, 28.
[7] B. Sharma, R. R. Frontiera, A.-I. Henry, E. Ringe, R. P. Van Duyne, *Mater. Today* **2012**, *15*, 16.
[8] N. Liu, M. Mesch, T. Weiss, M. Hentschel, H. Giessen, *Nano Lett.* **2010**, *10*, 2342.
[9] J. N. Anker, W. P. Hall, O. Lyandres, N. C. Shah, J. Zhao, R. P. Van Duyne, *Nat. Mater.* **2008**, *7*, 442.
[10] K. C. Bantz, A. F. Meyer, N. J. Wittenberg, H. Im, Ö. Kurtulus, S. H. Lee, N. C. Lindquist, S.-H. Oh, C. L. Haynes, *Phys. Chem. Chem. Phys.* **2011**, *13*, 11551.
[11] R. Bardhan, S. Lal, A. Joshi, N. J. Halas, *Acc. Chem. Res.* **2011**, *44*, 936.
[12] O. Neumann, A. S. Urban, J. Day, S. Lal, P. Nordlander, N. J. Halas, *ACS Nano* **2013**, *7*, 42.
[13] J. G. Smith, J. A. Faucheaux, P. K. Jain, *Nano Today* **2015**, *10*, 67.
[14] L. Zhou, Y. Tan, J. Wang, W. Xu, Y. Yuan, W. Cai, S. Zhu, J. Zhu, *Nat. Photonics* **2016**, *10*, 393.
[15] S. Linic, P. Christopher, D. B. Ingram, *Nat. Mater.* **2011**, *10*, 911.
[16] Z. Zheng, W. Xie, B. Huang, Y. Dai, *Chem., A Eur. J.* **2018**, *24*, 18322.
[17] P. R. West, S. Ishii, G. V. Naik, N. K. Emani, V. M. Shalaev, A. Boltasseva, *Laser Photon. Rev.* **2010**, *4*, 795.
[18] G. V. Naik, V. M. Shalaev, A. Boltasseva, *Adv. Mater.* **2013**, *25*, 3264.
[19] W. A. Murray, W. L. Barnes, *Adv. Mater.* **2007**, *19*, 3771.
[20] Y. Cui, A. Lauchner, A. Manjavacas, F. J. García De Abajo, N. J. Halas, P. Nordlander, *Nano Lett.* **2016**, *16*, 6390.
[21] A. Lauchner, A. E. Schlather, A. Manjavacas, Y. Cui, M. J. Mcclain, G. J. Stec, F. J. García De Abajo, P. Nordlander, N. J. Halas, *Nano Lett.* **2015**, *15*, 6208.
[22] T.-C. Hung, B. Kiraly, J. H. Strik, A. A. Khajetoorians, D. Wegner, *Nano Lett.* **2021**, *21*, 5006.
[23] C. Ayala-Orozco, D. Galvez-Aranda, A. Corona, J. M. Seminario, R. Rangel, J. N. Myers, J. M. Tour, *Nat. Chem.* **2023**. https://doi.org/10.1038/s41557-023-01383-y.
[24] C. Ayala-Orozco, C. Urban, M. W. Knight, A. S. Urban, O. Neumann, S. W. Bishnoi, S. Mukherjee, A. M. Goodman, H. Charron, T. Mitchell, M. Shea, R. Roy, S. Nanda, R. Schiff, N. J. Halas, A. Joshi, *ACS Nano* **2014**, *8*, 6372.
[25] C. Shirata, J. Kaneko, Y. Inagaki, T. Kokudo, M. Sato, S. Kiritani, N. Akamatsu, J. Arita, Y. Sakamoto, K. Hasegawa, N. Kokudo, *Sci. Rep.* **2017**, *7*, 13958.
[26] J. Yu, D. Javier, M. A. Yaseen, N. Nitin, R. Richards-Kortum, B. Anvari, M. S. Wong, *J. Am. Chem. Soc.* **2010**, *132*, 1929.
[27] S. Chen, L. Zhu, Z. Du, R. Ma, T. Yan, G. Alimu, X. Zhang, N. Alifu, C. Ma, *RSC Adv.* **2021**, *11*, 20850.
[28] H. I. Ingólfsson, M. N. Melo, F. J. Van Eerden, C. Arnarez, C. A. Lopez, T. A. Wassenaar, X. Periole, A. H. De Vries, D. P. Tieleman, S. J. Marrink, *J. Am. Chem. Soc.* **2014**, *136*, 14554.
[29] P. S. Niemelä, S. Ollila, M. T. Hyvönen, M. Karttunen, I. Vattulainen, *PLoS Comput. Biol.* **2007**, *3*, e34.
[30] F. Li, C. U. Chan, C. D. Ohl, *Biophys. J.* **2013**, *105*, 872.
[31] E. Evans, B. A. Smith, *New J. Phys.* **2011**, *13*, 095010.
[32] T. Shigematsu, K. Koshiyama, S. Wada, *Sci. Rep.* **2015**, *5*, 15369.
[33] S. Gil-Guerrero, Á. Peña-Gallego, M. Mandado, *J. Phys. Chem. C* **2019**, *124*, 1585.

[34] L. Shao, C. Fang, H. Chen, Y. C. Man, J. Wang, H.-Q. Lin, *Nano Lett.* **2012**, *12*, 1424.
[35] A. Mishra, R. K. Behera, P. K. Behera, B. K. Mishra, G. B. Behera, *Chem. Rev.* **2000**, *100*, 1973.
[36] C. Shi, J. B. Wu, D. Pan, *J. Biomed. Opt.* **2016**, *21*, 050901.
[37] M. Falabella, H. J. Vernon, M. G. Hanna, S. M. Claypool, R. D. S. Pitceathly, *Trends Endocrinol. Metab.* **2021**, *32*, 224.
[38] H. H. Szeto, *Br. J. Pharmacol.* **2014**, *171*, 2029.
[39] A. J. Chicco, G. C. Sparagna, *Am. J. Physiol., Cell Physiol.* **2007**, *292*, C33.
[40] J. Sangster, *J. Phys. Chem. Ref. Data* **2009**, *18*, 1111.
[41] E. A. Tehrany, F. Fournier, S. Desobry, *J. Food Eng.* **2004**, *64*, 315.
[42] G. Majno, I. Joris, *Am. J. Pathol.* **1995**, *146*, 3.
[43] S. L. Fink, B. T. Cookson, *Infect. Immun.* **2005**, *73*, 1907.
[44] R. Zhang, L. Bursi, J. D. Cox, Y. Cui, C. M. Krauter, A. Alabastri, A. Manjavacas, A. Calzolari, S. Corni, E. Molinari, E. A. Carter, F. J. García De Abajo, H. Zhang, P. Nordlander, *ACS Nano* **2017**, *11*, 7321.
[45] L. Bursi, A. Calzolari, S. Corni, E. Molinari, *ACS Photonics* **2016**, *3*, 520.
[46] A. L. Santos, D. Liu, A. K. Reed, A. M. Wyderka, A. Van Venrooy, J. T. Li, V. D. Li, M. Misiura, O. Samoylova, J. L. Beckham, C. Ayala-Orozco, A. B. Kolomeisky, L. B. Alemany, A. Oliver, G. P. Tegos, J. M. Tour, *Sci. Adv.* **2022**, *8*, eabm2055.
[47] A. L. Santos, J. L. Beckham, D. Liu, G. Li, A. Van Venrooy, A. Oliver, G. P. Tegos, J. M. Tour, *Adv. Sci.* **2023**, *10*, 2205781.
[48] J. L. Beckham, A. R. Van Venrooy, S. Kim, G. Li, B. Li, G. Duret, D. Arnold, X. Zhao, J. T. Li, A. L. Santos, G. Chaudhry, D. Liu, J. T. Robinson, J. M. Tour, *Nat. Nanotechnol.* **2023**, *18*, 1051.